

# Design of a Low-Cost, Lightweight, Passively Cooled, Narrowband, SWIR Camera for Space-Based Imaging

5 July 2003

Prepared by

R. J. RUDY, Y. DOTAN, J. H. HECHT,  
D. J. MABRY, and M. G. SIVJEE  
Space Science Applications Laboratory  
Laboratory Operations

D. W. WARREN  
Sensor Systems Subdivision  
Electronic Systems Division

Prepared for

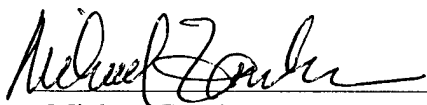
SPACE AND MISSILE SYSTEMS CENTER  
AIR FORCE SPACE COMMAND  
2430 E. El Segundo Boulevard  
Los Angeles Air Force Base, CA 90245

Engineering and Technology Group

This report was submitted by The Aerospace Corporation, El Segundo, CA 90245-4691, under Contract No. F04701-00-C-0009 with the Space and Missile Systems Center, 2430 E. El Segundo Blvd., Los Angeles Air Force Base, CA 90245. It was reviewed and approved for The Aerospace Corporation by J. A. Hackwell, Principal Director, Space Science Applications Laboratory; and I. Ghozeil, Principal Director, Sensor Systems Subdivision. Michael Zambrana was the project officer for the Mission-Oriented Investigation and Experimentation (MOIE) program.

This report has been reviewed by the Public Affairs Office (PAS) and is releasable to the National Technical Information Service (NTIS). At NTIS, it will be available to the general public, including foreign nationals.

This technical report has been reviewed and is approved for publication. Publication of this report does not constitute Air Force approval of the report's findings or conclusions. It is published only for the exchange and stimulation of ideas.

A handwritten signature in black ink, appearing to read "Michael Zambrana", is written over a horizontal line.

Michael Zambrana  
SMC/AXE

REPORT DOCUMENTATION PAGE			Form Approved OMB No. 0704-0188	
Public reporting burden for this collection of information is estimated to average 1 hour per response, including the time for reviewing instructions, searching existing data sources, gathering and maintaining the data needed, and completing and reviewing this collection of information. Send comments regarding this burden estimate or any other aspect of this collection of information, including suggestions for reducing this burden to Department of Defense, Washington Headquarters Services, Directorate for Information Operations and Reports (0704-0188), 1215 Jefferson Davis Highway, Suite 1204, Arlington, VA 22202-4302. Respondents should be aware that notwithstanding any other provision of law, no person shall be subject to any penalty for failing to comply with a collection of information if it does not display a currently valid OMB control number. PLEASE DO NOT RETURN YOUR FORM TO THE ABOVE ADDRESS.				
1. REPORT DATE (DD-MM-YYYY) 05-07-2003		2. REPORT TYPE		3. DATES COVERED (From - To)
4. TITLE AND SUBTITLE  Design of a Low Cost, Lightweight, Passively-cooled, Narrowband, SWIR Camera for Space-based Imaging		5a. CONTRACT NUMBER F04701-00-C-0009		
		5b. GRANT NUMBER		
		5c. PROGRAM ELEMENT NUMBER		
6. AUTHOR(S)  R, J. Rudy, Y. Dotan, J. H. Hecht, D. J. Mabry, M. G. Sivjee, D. W. Warren		5d. PROJECT NUMBER		
		5e. TASK NUMBER		
		5f. WORK UNIT NUMBER		
7. PERFORMING ORGANIZATION NAME(S) AND ADDRESS(ES)  The Aerospace Corporation Laboratory Operations El Segundo, CA 90245-4691		8. PERFORMING ORGANIZATION REPORT NUMBER  TR-2003(8570)-10		
9. SPONSORING / MONITORING AGENCY NAME(S) AND ADDRESS(ES) Space and Missile Systems Center Air Force Space Command 2450 E. El Segundo Blvd. Los Angeles Air Force Base, CA 90245		10. SPONSOR/MONITOR'S ACRONYM(S) SMC		
		11. SPONSOR/MONITOR'S REPORT NUMBER(S) SMC-TR-03-20		
12. DISTRIBUTION/AVAILABILITY STATEMENT  Approved for public release; distribution unlimited.				
13. SUPPLEMENTARY NOTES				
14. ABSTRACT  This document describes the conceptual design for a spaceborne imager operating in the short-wave infrared (SWIR). The instrument was designed to image a single emission line of OH from the night sky from a satellite in low Earth orbit, but much of the design is relevant to other imaging applications. The imager has a 23.4° FOV in the cross-track direction with a resolution of 1.6 mrad. It functions like a line scanner but incorporates a two-dimensional (256 x 256) InGaAs focal-plane array (FPA) to attain high signal-to-noise. It employs a set of telecentric foreoptics to accommodate narrowband imaging, but a simpler design would serve for broadband measurements. It uses a small radiator to passively cool the FPA to < 200K and direct radiation by the support assembly to reduce the temperature of the optics. A novel approach that accomplishes TDI (time, delay, integrate) off of the focal plane obviates the need for a step/stare mirror. The design has no moving parts, weighs less than 6 kg, and consumes less than 15 W of power.				
15. SUBJECT TERMS  Space instrumentation, Infrared imaging, Infrared radiometry				
16. SECURITY CLASSIFICATION OF:			17. LIMITATION OF ABSTRACT	18. NUMBER OF PAGES  15
a. REPORT UNCLASSIFIED	b. ABSTRACT UNCLASSIFIED	c. THIS PAGE UNCLASSIFIED		
				19a. NAME OF RESPONSIBLE PERSON Richard Rudy
				19b. TELEPHONE NUMBER (include area code) (310)336-5799

## **Acknowledgments**

We wish to thank Dr. J. Kumer of the Lockheed Martin Advanced Technology Center for several helpful discussions and to B. Weissbard and M. Farris of the Rockwell Science Center for information on infrared focal-plane arrays. This work was supported by the US Air Force Space and Missile Systems Center through the Mission-Oriented Investigation and Experimentation program, under contract F4701-00-C-0009.

## Contents

1. Background .....	1
2. Selection of the Focal-Plane Array .....	3
3. Optical Design.....	5
4. Mechanical Design .....	9
5. Electronics.....	13
6. Summary .....	15

## Figures

1. Optical layout SWIR imager.....	7
2. Spot diagrams for the entire optical train.....	7
3. Opto-mechanical design.....	9
4. Schematic of the electrical design.....	13

## Tables

1. Dark Current as a Function of Temperature for a 40 $\mu\text{m}$ InGaAs Pixel with a Cutoff Wavelength of 1.7 $\mu\text{m}$ .....	3
2. Wavelength Shifts as a Function of the Angle of Incidence for a Filter Centered at 1.4 $\mu\text{m}$ on a Glass Substrate.....	5
3. Component and Total Weights for Imager .....	10
4. FPA Temperature as a Function of Radiator Emissivity.....	11

## 1. Background

The history of this project is very brief. Approximately 6 weeks prior to the proposal deadline, Aerospace was approached about providing an instrument for a NASA Small Explorer (SMEX) class mission. The instrument needed to image the nighttime mesospheric hydroxyl (OH) emission at  $1.4\ \mu\text{m}$  from a 550-km orbit. The instrument was severely weight limited ( $<6\ \text{kg}$ ) and had tight restrictions on both power (15 W) and cost (\$2.6 M). It needed to provide a reasonable field of view (FOV) at good spatial resolution ( $<2\ \text{km}$ ) and high signal-to-noise ( $S/N \geq 100$ ) with significant processing capability to keep the data flow manageable. In addition to observing the OH emission in a single bright emission line, the system also needed to sample the background emission in a second nearby band that was free of OH. The design that resulted from these requirements is described below.

## 2. Selection of the Focal-Plane Array

The choice of the focal-plane array (FPA) was the first, and in some ways most fundamental, decision to be made. Many aspects of the optical design flowed from the linear dimensions and pixel pitch of the FPA. The stringent performance dictated by the mission requirements limit the commercially available FPAs to only a few units. The  $1.4\text{ }\mu\text{m}$  operating wavelength precluded the use of intrinsic silicon (CCDs or CMOS) detectors. InSb was ruled out because its very long cut-off wavelength ( $>5\text{ }\mu\text{m}$ ) leads to overwhelmingly large dark currents and background fluxes at the operating temperatures envisioned.

The two detector materials that remained as possible candidates were HgCdTe and InGaAs. Both are ternary compounds that can have the relative proportions of the three materials varied to cover a broad range of wavelengths. Typically, there is a short-wave cutoff at wavelengths  $< 1\text{ }\mu\text{m}$  due to absorption in the material. The long-wave cutoff is selected by choosing the proper material proportions. Photons below a certain energy (and thus beyond a certain wavelength) will not promote charges into a conduction band where they can be detected. The general rule of thumb is to tailor the bandgap such that the cutoff wavelength is just to the red of the longest wavelength for which a detection is required. This is extremely important in situations where cooling capacity is limited since by maximizing the bandgap the thermally generated charges in the detector material (the so-called dark current) are minimized. Moreover, a larger bandgap and a shorter cutoff wavelength also minimize the detection of unwanted thermal background from the detector housing, optics, filters, etc. Thus for this program with measurement requirements at  $1.4\text{ }\mu\text{m}$ , a cutoff wavelength of  $\sim 1.5\text{ }\mu\text{m}$  would seem ideal. In actuality, neither HgCdTe nor InGaAs exist in a broad assortment of cutoff wavelengths. Other than a few "standard" cutoffs, other wavelengths require a development effort that is beyond the budget of this program. For that reason, we considered both materials with cutoff wavelengths of  $1.7\text{ }\mu\text{m}$ , a value for which the vendors either had assets or a good deal of experience in growing reliable detector material. At Rockwell's recommendation, we selected InGaAs as the detector material since it exhibits smaller dark currents over the range of temperatures that the FPA is likely to operate with comparable or better quantum efficiency than HgCdTe. Table 1 presents the dark current as a function of temperature as derived from some test data provided by Rockwell.

Table 1. Dark Current as a Function of Temperature for a  $40\text{ }\mu\text{m}$  InGaAs Pixel with a Cutoff Wavelength of  $1.7\text{ }\mu\text{m}$ .

Temperature (K)	Dark Current (electrons $\text{sec}^{-1}$ @ 50 mV bias)
170	0.003
180	0.1
190	1.6
200	16
210	160
220	1280

After deciding on InGaAs as the detector material, the single remaining decision was the selection of the multiplexor (MUX). There were two, again supplied by the Rockwell Science Center, that met the low read noise criterion necessary to satisfy the signal-to-noise requirement. These were the Hawaii MUX with  $18.5\text{ }\mu\text{m}$  pixels in a  $1024 \times 1024$  format and the PICNIC MUX with  $40\text{ }\mu\text{m}$  pixels in a  $256 \times 256$  arrangement. While the former would have produced a more capable instrument, problems with reading the array sufficiently rapidly to keep pace with the satellite motion and the processing required to handle the large number of pixels, plus a significantly greater cost, led us to choose the PICNIC MUX instead. The operation of this resulting InGaAs array on the  $256 \times 256$  PICNIC MUX is discussed further in the electronics section.



### 3. Optical Design

Once the FPA had been selected the remaining factors that drove the optical design were field of view (FOV), footprint size, and signal-to-noise (S/N). An additional consideration was the necessity to observe with a second background filter in addition to a narrowband filter that isolates a strong OH emission line.

The FOV and footprint size are related by the fact that, for utilization of the full array, the FOV is 256 times the footprint. For this reason the two were considered together. In choosing the FOV, it was desirable to have sufficient spatial coverage in the cross-track (the direction perpendicular to the motion of the spacecraft) to resolve the largest of the atmospheric wave structures that the mission targeted. Coverage in this direction of 23.4° provided 190 km at the level of the OH emission, sufficient to fulfill this goal. This corresponded to a footprint of 0.74 km, well under the 2-km resolution necessary to investigate wave activity on the smallest scales.

Before considering the S/N requirement, a topic that will also be discussed in the electronics section, we consider the requirement for narrowband imaging and how this affects the optical design. The issue is that the effective passband of a filter changes as the angle of the incident light varies. The shift in wavelength, which is always towards shorter wavelengths, can, for small angles, be expressed as:

$$\Delta\lambda = \lambda\theta^2/2n^2,$$

where  $\theta$  is the angle from normal, and  $n$  is the index of refraction of the substrate.

Table 2 presents shifts for a range of incidence angles for a bandpass centered at 1.4344  $\mu\text{m}$ , the location of the OH line of interest. The values were computed for an index of refraction of 1.57, a

Table 2. Wavelength Shifts as a Function of the Angle of Incidence for a Filter Centered at 1.4  $\mu\text{m}$  on a Glass Substrate

Angle of Incidence (°)	Wavelength Shift (Å)
0.0	0.0
1.0	0.87
2.0	3.48
2.86	7.11
4.0	13.9
8.0	55.7
10.0	87.0
11.7	119

value representative of several common glasses. Since the anticipated width of the bandpass is only  $\sim 13\text{\AA}$ , an angle of incidence greater than  $4^\circ$  will shift the bandpass off of the emission line. Since the  $23.4^\circ$  FOV implies a maximum, off-normal angle of  $23.4^\circ/2 = 11.7^\circ$ , it is apparent from Table 2 that the optical design could not simply place the filter in front of the optics. In fact, the situation is considerably more restrictive than this. Because it is necessary to compare very precisely different regions of the FOV with each other, each region of the FOV needs to be transmitted by the filter in precisely the same manner.

The solution to both these problems is to form a telecentric image of the field for passage through the filter. Telecentric images have the property that light bundles from all parts of the fields are parallel. This means that every portion of the field is affected by the filter in the same way. The problem relating to the angle of incidence is addressed by expanding the size of the telecentric image. This has the corresponding effect of making the spread of the light bundles (the f-cones) small. For  $f/10$  beams, the largest off-normal angle is  $2.86^\circ$ . From Table 2 it can be seen that this produces a wavelength shift of only a little over  $7\text{\AA}$ , which is acceptable for a  $13\text{\AA}$  bandpass.

Figure 1 shows the optical design. The first three lenses (to the left side) provide the light-gathering aperture necessary to meet the signal-to-noise requirements as well as encompassing the large FOV. They also form the telecentric image of the FOV. The filters (not shown), which are co-planar and butted together, are positioned very near the telecentric focus. As noted above, by producing a comparatively large image at the telecentric focus, the f-cones for each part of the field are kept narrow.

The remaining five lenses (to the right of the telecentric focus) de-magnify and re-image the field on the FPA. The reduction in image size is considerable, taking the field that is approximately 2 in. on a side and re-imaging it on a 1-cm-square detector. The FOV is split evenly between the two filters, with each covering the full width of the track (i.e., a given point in the OH layer is imaged sequentially by the two filters as the spacecraft moves the location through the FOV). Figure 2 shows the spot sizes produced by this optical design. As can be seen, for both wavelengths and for all portions of the field, the spot sizes are much smaller than a single pixel.

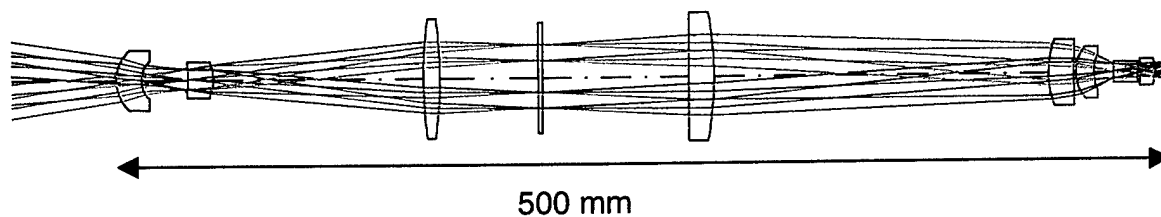


Figure 1. Optical layout SWIR imager.

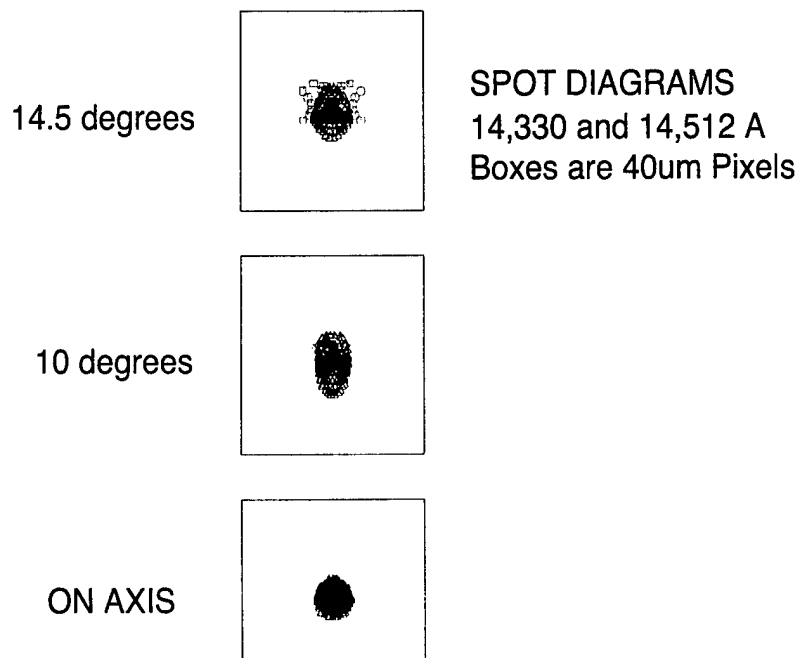


Figure 2. Spot diagrams for the entire optical train. The boxes show the size of a 40- $\mu\text{m}$  pixel. The blue shows the spots at the wavelength of the OH line (1.4344  $\mu\text{m}$ ); the red shows some small additional spread at the wavelength of the background filter (1.4503  $\mu\text{m}$ ).

The optics that produced these very small spots are all composed of a single glass—LAH58. It is a very dense glass and was selected to see if the optical design could be implemented in a heavy material and still meet the weight requirements. If the material needed to be changed there is now every assurance that we remain within the limit.

#### 4. Mechanical Design

The mechanical design had to accommodate the optical design by allowing for the precise positioning and mounting of the optics while housing and cooling the detector. Moreover, it had to accomplish this while meeting the stringent weight allotment. Figure 3 shows the mechanical design. The all-refractive optics make possible a very simple design in which all optical elements are mounted along a

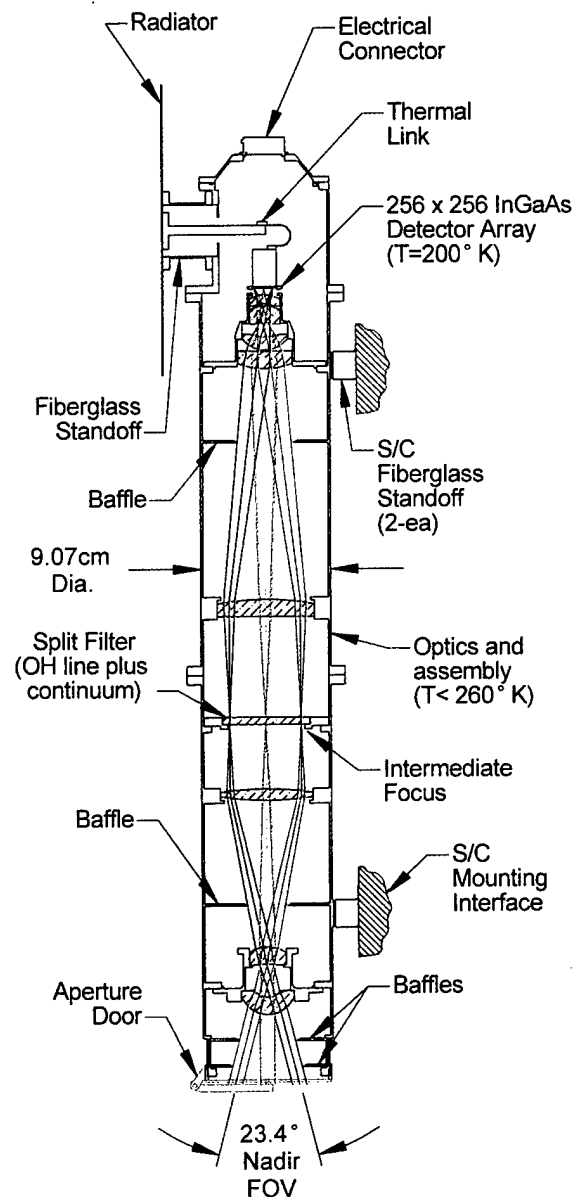


Figure 3. Opto-mechanical design.

single axis in a tube-like structure. To facilitate construction, the structure has three separate sections. The first contains the lenses that form the intermediate telecentric image and the filters. The second supports the five lenses that re-image the field on the detector. The final portion houses the detector, its mount, and the attendant cabling and provides for the thermal link to the radiator. Wherever possible, the optics are baffled to limit stray light. The tube structure has a wall thickness of 60 mils.

Weight restrictions dictated that the tube structure be aluminum, beryllium, or composite. Cost narrowed this to aluminum. Table 3 lists the design weights. Note that the total is < 6 kg.

As noted in the FPA section and evident in Table 1, the FPA must be cooled below ambient temperature to keep the dark current tractable. Weight, cost, and power restrictions preclude the use of a cryocooler. Temperatures near the desired range (<200K) are just barely obtainable with a two-stage thermoelectric cooler and this remains a viable alternative. We have selected radiative (passive) cooling as our baseline, however. Assuming that a radiator is shielded from both the sun and the Earth and has an unobstructed view of deep space, it is warmed only by zodiacal light and diffuse galactic emission, and its temperature may fall as low as ~30K. For objects in low Earth orbit, however, the principal limitation on radiator temperature becomes heat loading from the spacecraft, both conductive and radiative. If the radiator is attached to the spacecraft by a material of low thermal conductivity, radiation from the spacecraft becomes the dominant heating mechanism. Table 4 presents the predicted focal-plane temperatures as a function of the radiative coupling between the radiator and the spacecraft. It assumes a radiator with an area of 50 in.<sup>2</sup>, an effective emissivity of 0.8 radiating to space (this low value allows for some degradation over the life of the mission), a spacecraft temperature of 300K, <1 mW of heat dissipation by the FPA, 46 mW of radiative loading on the FPA and cooling link, and mounting of the radiator to the spacecraft with a 1-in.-dia tube of G10 with a 50-mil wall thickness and a 1-in. length. Conduction through the latter is second to the radiative load from the spacecraft in heating the radiator, but in all cases contributes less than 30% of the load.

Table 3. Component and Total Weights for Imager

Component	lbs.	kg
Optics (no filter)	1.136	0.515
Filter (5mm thick)	0.134	0.050
Electronics box	5.280	2.395
cards	2.700	1.225
enclosure	2.580	1.170
connectors	0.1	0.045
cable (conns./shielding)	0.15	0.068
Detector mount assembly	0.260	0.118
Radiator assembly	0.250	0.113
Aperture Door Assy	0.200	0.091
Structure and mounts	4.256	1.930
Total	11.75	5.34

Table 4. FPA Temperature as a Function of Radiator Emissivity. This is the emissivity of the side facing the spacecraft. It determines the radiative coupling between the spacecraft and the radiator, which is the principal heat load on the radiator.

Emissivity	FPA Temperature (K)
0.05	161.9
0.075	172.9
0.10	181.7
0.15	195.3
0.20	205.6

While a value of  $< 0.05$  for the emissivity should be readily obtainable with a gold overcoating to the aluminum plate radiator, a radiative barrier composed of a highly reflective plate will be inserted between the radiator and the spacecraft. This serves the same purpose as multi-layer-insulation (MLI) and will be helpful in achieving the very low effective emissivity. To reduce any thermally generated background from the optics themselves, the temperature of the entire assembly is lowered to  $\sim 250\text{K}$  using passive cooling. For this reason the instrument is mounted in a shaded region on the outside wall of the spacecraft.

## 5. Electronics

The electronics generate the clocks and bias voltages that operate the FPA; and amplify, digitize, and record the analog signals that are produced by it. Moreover, the electronics provide for an effective, off-chip TDI (time, delay, and integrate) that is necessary to achieve the requisite signal-to-noise. The implementation of all of these functions is accomplished via four separate, custom circuit cards that are shown schematically in Figure 4.

Cards 1 and 3 provide the interface with the FPA—card 3 creates the timing signals and voltages necessary to operate and sequence the array while card 1 accepts the output signal and performs the amplification before passing the signals to the single analog-to-digital converter (ADC). The decision to multiplex the four FPA outputs to a single ADC was necessary because of the large power consumption of the ADC. Card number 4 conditions and isolates the instrument power from the spacecraft power while card 2 communicates the measurements to the spacecraft for telemetry to Earth

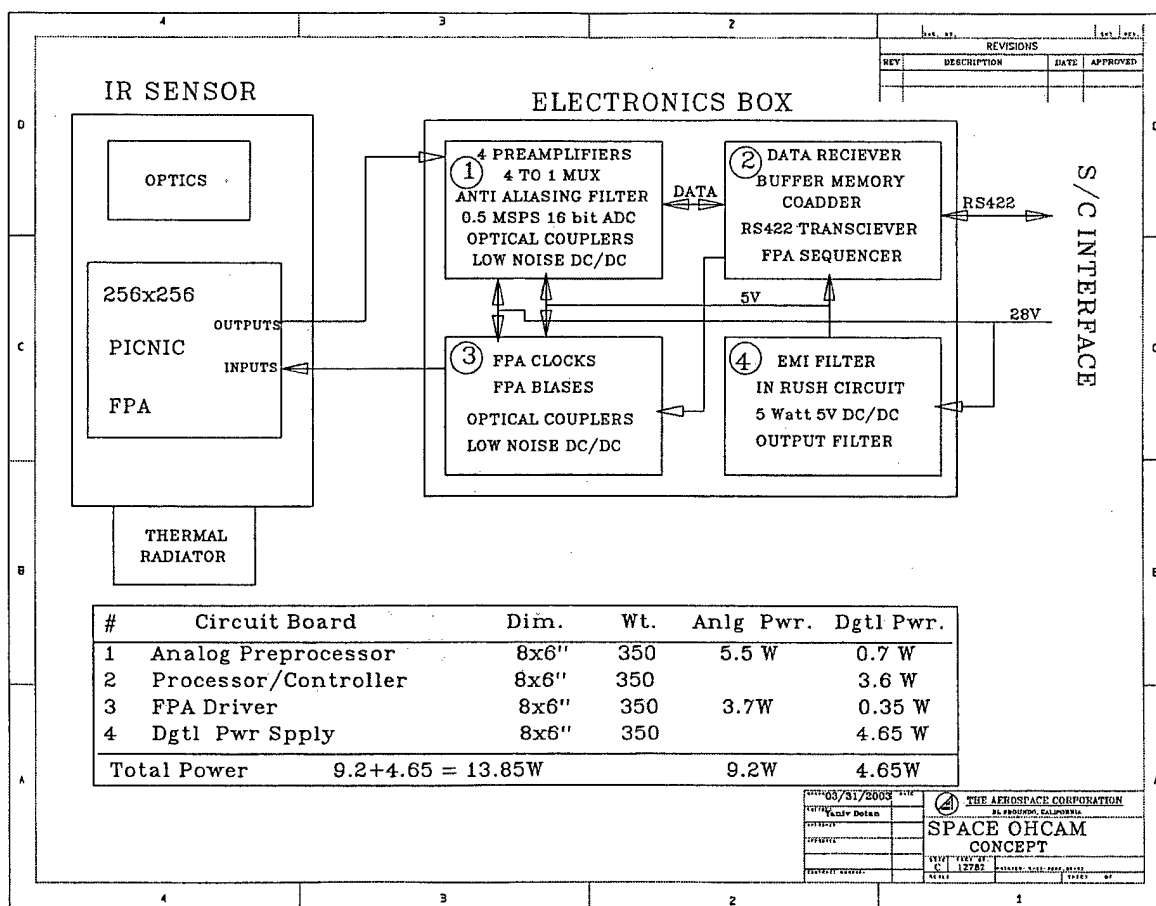


Figure 4. Schematic of the electrical design.

after first performing the crucial TDI processing. The latter removes the need for expensive "step and stare" mechanisms in front of the optics and is described in some detail in the following paragraph.

True TDI is associated with CCDs (charge coupled devices) and results from the ability to transfer the photo-generated charge from one pixel to another. The rate at which the charge is transferred can be chosen to offset image motion, thereby allowing the integration time on an area of interest in the FOV to be as long as the time it takes that area to transit the array. Because the PICNIC array (like most infrared arrays) has separate circuitry for each pixel that is not linked to the other pixels, TDI as implemented on CCDs is not possible. What is possible, and what is intended for this instrument, is to read the array at the frame rate that matches the motion of the image from one row of the array to the next and to coadd these frames in such a manner as to keep track of the image motion and preserve the resolution of a single pixel. Since this will involve the coaddition of from 64 to 96 frames, the "trick" is to minimize the read noise. To do so, we make use of the fact that the read noise is associated almost entirely with the reset process (the process by which a pixel is switched to ground to clear the charge that has accumulated) and not with the actual sampling of the array. For this reason, it is our intent to reset the array only a single time during the 64 to 96 frames that constitute a measurement cycle. This is, of course, only possible if the photo-charge does not exceed the integration capacity of a pixel. The light levels anticipated fill only a quarter to a third of this capacity so the observing conditions are comfortably within that limit. Without the reset, however, the photo-charge continues to accrue. Thus the signal measured for a given pixel during a given frame must have its value from the prior frame subtracted from it.



## 6. Summary

This document has presented the conceptual design for a very lightweight ( $<6$  kg), low-power ( $<15$  W), passively cooled, low-cost ( $\sim \$2.5$ M), spaceborne SWIR imager. The instrument was designed for a NASA proposal to image a single emission line of OH from the night sky from a satellite in low Earth orbit, but much of the design has broad applicability. The imager has a  $23.4^\circ$  FOV in the cross-track direction with a resolution of 1.6 mrad. The heart of the imager is a modern  $256 \times 256$  InGaAs FPA. It is operated in a "pushbroom" fashion, but instead of employing a single line of detectors, utilizes most of its rows to enhance signal-to-noise. A sophisticated set of electronics performs the necessary shifting, sorting, and coadding necessary to preserve the spatial resolution of a single pixel.

## ELECTRONIC SYSTEMS DIVISION

The Electronic Systems Division provides world-class leadership in space-related electronic systems, ensuring that our national-security, civil, and commercial customers have the tools to conceive, develop, and operate successful, operationally integrated, and cost-effective space systems.

Engineering and scientific expertise includes satellite and terrestrial communications, remote sensing, and spaceborne electronics and evaluation. Our experienced staff and extensive laboratory facilities provide a unique and complete package of end-to-end engineering and scientific support in all areas related to space-system electronics. The skills mix ranges from rare specialties to broad technical and programmatic knowledge and experience. The three subdivisions of the Electronic Systems Division have unique but intertwined functions. Together they cover all aspects related to space and supporting ground electronics and electronic systems.

**Electronics Engineering Subdivision:** Provides experience in space-system electronics engineering, from the microelectronics piece-part level to the launch-vehicle and satellite electronic subsystem and system level. This experience is applied to electronics design; modeling and simulation; rapid prototyping; parts management; failure analysis; anomaly resolution; power systems engineering; and subsystem architecture assessments.

**Sensor Systems Subdivision:** Provides resources for electromagnetic radiation ranging from ultraviolet to longwave radio frequencies. These resources are applied to the design, analysis, simulation, and modeling of a variety of remote-sensing systems, from active radiators such as radar to such passive radiators as weather sensors. In-depth knowledge and experience with the operation of these systems, as well as the exploitation and application of the sensor data, are also available.

**Communication Systems Subdivision:** Provides knowledge spanning the full range of communication technologies and applications, including spectrum management and communication system architectures; analysis of data communication and telemetry, command, and control links; and specialized hardware and software for the implementation of space and terrestrial communication systems.

## LABORATORY OPERATIONS

The Aerospace Corporation functions as an "architect-engineer" for national security programs, specializing in advanced military space systems. The Corporation's Laboratory Operations supports the effective and timely development and operation of national security systems through scientific research and the application of advanced technology. Vital to the success of the Corporation is the technical staff's wide-ranging expertise and its ability to stay abreast of new technological developments and program support issues associated with rapidly evolving space systems. Contributing capabilities are provided by these individual organizations:

**Electronics and Photonics Laboratory:** Microelectronics, VLSI reliability, failure analysis, solid-state device physics, compound semiconductors, radiation effects, infrared and CCD detector devices, data storage and display technologies; lasers and electro-optics, solid-state laser design, micro-optics, optical communications, and fiber-optic sensors; atomic frequency standards, applied laser spectroscopy, laser chemistry, atmospheric propagation and beam control, LIDAR/LADAR remote sensing; solar cell and array testing and evaluation, battery electrochemistry, battery testing and evaluation.

**Space Materials Laboratory:** Evaluation and characterizations of new materials and processing techniques: metals, alloys, ceramics, polymers, thin films, and composites; development of advanced deposition processes; nondestructive evaluation, component failure analysis and reliability; structural mechanics, fracture mechanics, and stress corrosion; analysis and evaluation of materials at cryogenic and elevated temperatures; launch vehicle fluid mechanics, heat transfer and flight dynamics; aerothermodynamics; chemical and electric propulsion; environmental chemistry; combustion processes; space environment effects on materials, hardening and vulnerability assessment; contamination, thermal and structural control; lubrication and surface phenomena. Microelectromechanical systems (MEMS) for space applications; laser micromachining; laser-surface physical and chemical interactions; micropropulsion; micro- and nanosatellite mission analysis; intelligent microinstruments for monitoring space and launch system environments.

**Space Science Applications Laboratory:** Magnetospheric, auroral and cosmic-ray physics, wave-particle interactions, magnetospheric plasma waves; atmospheric and ionospheric physics, density and composition of the upper atmosphere, remote sensing using atmospheric radiation; solar physics, infrared astronomy, infrared signature analysis; infrared surveillance, imaging and remote sensing; multispectral and hyperspectral sensor development; data analysis and algorithm development; applications of multispectral and hyperspectral imagery to defense, civil space, commercial, and environmental missions; effects of solar activity, magnetic storms and nuclear explosions on the Earth's atmosphere, ionosphere and magnetosphere; effects of electromagnetic and particulate radiations on space systems; space instrumentation, design, fabrication and test; environmental chemistry, trace detection; atmospheric chemical reactions, atmospheric optics, light scattering, state-specific chemical reactions, and radiative signatures of missile plumes.